$^{99m}$Tc-antifibrin Fab' fragments for imaging venous thrombi: evaluation in a canine model. *Radiology* 1989;173:163–169.
18. Knight LC, Abrams MJ, Schwartz DA, Hauser MM, Kollman M, Gaul FE, Rauh DA. Preparation and preliminary evaluation of technetium-99m-labeled Fragment $E_1$ for thrombus imaging. *J Nucl Med* 1992;33:710–715.
19. Becker W, Borner W, Borst U. Technetium-99m-hexamethylpropyleneamineoxime (HMPAO) as a platelet label: evaluation of labeling parameters and first in vivo results. *Nucl Med Commun* 1988;9:831–842.
20. Freiman DG. The structure of thrombi. In: Coleman R, Hirsh J, Marder V, Salzman E, eds. *Hemostasis and thrombosis. Basic principles and clinical practice*, 2nd ed. Philadelphia: JB Lippincott Co.; 1987:1123–1135.
21. Coller BS. Activation affects access to the platelet receptor for adhesive glycoproteins. *J Cell Biol* 1986;103:451–456.
22. Plow EF, Pierschbacher MD, Ruoslahti E, Marguerie GA, Ginsberg MH. The effect of Arg-Gly-Asp-containing peptides on fibrinogen and von Willebrand factor binding to platelets. *Proc Natl Acad Sci USA* 1985;82:8057–8061.
23. Samanen J, Ali F, Romoff T, et al. Development of a small RGD peptide fibrinogen receptor antagonist with potent antiaggregatory activity in vitro. *J Med Chem* 1991;34:3114–3125.
24. Alig L, Edenhofter A, Hadvary P, et al. Low molecular weight, nonpeptide fibrinogen receptor antagonists. *J Med Chem* 1992;35:4393–4407.
25. Zablocki JA, Miyano M, Garland RB, et al. Potent in vitro and in vivo inhibitors of platelet aggregation based upon the Arg-Gly-Asp-Phe sequence of fibrinogen. A proposal on the nature of the binding interaction between the Arg-guanidine of RGDX mimetics and the platelet GP IIb/IIIa receptor. *J Med Chem* 1993;36:1811–1819.
26. Cook NS, Bruttger O, Pally C, Hagenbach A. The effects of two synthetic glycoprotein IIb/IIIa antagonists, Ro 43-8857 and L-700,462, on platelet aggregation and bleeding in guinea pigs and dogs: evidence that Ro 43-8857 is orally active. *Throm Haemostasis* 1993;70:838–847.
27. Ramjit DR, Lynch JJ, Sitko GR, et al. Antithrombotic effects of MK-0852, a platelet fibrinogen receptor antagonist, in canine models of thrombosis. *J Pharmacol Exp Ther* 1993;266:1501–1511.
28. Scarborough RM, Naughton A, Teng W, et al. Design of potent and specific integrin antagonists. *J Biol Chem* 1993;268:1066–1073.
29. Cheng S, Craig WS, Mullen D, Tschopp JF, Dixon D, Pierschbacker MD. Design and synthesis of novel cyclic RGD-containing peptides as highly potent and selective integrin $\alpha_{IIb}\beta_3$ antagonists. *J Med Chem* 1994;37:1–9.
30. Mousa SA, Bozarth JM, Forsythe MS, et al. Antiplatelet and antithrombotic efficacy of DMP 728, a novel platelet GPIIb/IIIa receptor antagonist. *Circulation* 1994;89:3–12.
31. Dennis MS, Henzel WJ, Pitti RM, et al. Platelet glycoprotein IIb/IIIa protein antagonists from snake venoms: evidence for a family of platelet-aggregation inhibitors. *Proc Natl Acad Sci USA* 1989;87:2471–2475.
32. Charo IF, Kieffer N, Phillips DR. Platelet membrane glycoproteins. In: Coleman R, Hirsh J, Marder V, Salzman E, eds. *Hemostasis and thrombosis. Basic principles and clinical Practice*, 3rd ed. Philadelphia: JB Lippincott Co.; 1994:489–507.
33. Muto P, Lastoria S, Varrella P, Vergara E, Bernardy JD, Borer JS, Salvatore M. Detection of deep venous thrombosis by technetium-99m-labeled synthetic peptides P-280: preliminary results. *J Nucl Med* 1994;34:80P.
34. Muto P, Lastoria S, Varrella P, et al. Detection of deep venous thrombosis with technetium-99m-labeled synthetic peptide P280. *J Nucl Med* 1995;36:1384–1391.



# Influence of Downscatter in Simultaneously Acquired Thallium-201/Technetium-99m-PYP SPECT

Hiroshi Ando, Takaya Fukuyama, Wataru Mitsuoka, Shogo Egashira, Yoshihiro Imamura, Hiroyuki Masaki and Toshiaki Ashihara

*Division of Cardiology, Matsuyama Red Cross Hospital, Matsuyama, Ehime, Japan*

Simultaneously acquired dual-isotope imaging is a unique and useful approach in SPECT. Photon spillover, however, is a potential limitation of this technique. **Methods:** To investigate the degree of $^{99m}$Tc downscatter into the $^{201}$Tl window in patients, simultaneously acquired dual-isotope $^{201}$Tl/$^{99m}$Tc-pyrophosphate imaging was performed in 17 patients with acute myocardial infarction (MI). Thallium-201 SPECT imaging was performed first, with a $^{201}$Tl photopeak window after the $^{201}$Tl injection (early $^{201}$Tl images), followed by $^{99m}$Tc injection and SPECT acquisition using dual-isotope windows (dual $^{201}$Tl images). Twenty-four hours after the $^{99m}$Tc injection, a third set of $^{201}$Tl images was obtained (24-hr $^{201}$Tl images). Thallium defect size (extent score) and defect severity (severity score) were calculated from these three sets of $^{201}$Tl images to quantify the MI. **Results:** Technetium-99m accumulation of varying intensity was recognized in all patients. Extent scores and severity scores were identical in early $^{201}$Tl images and 24-hr $^{201}$Tl images. Both scores, however, in the dual $^{201}$Tl images were decreased by 36% and 53%, respectively. **Conclusion:** There is a considerable $^{99m}$Tc downscatter into the $^{201}$Tl window, which prevents precise quantification of MI in simultaneously acquired dual-isotope $^{201}$Tl/$^{99m}$Tc-pyrophosphate imaging.

**Key Words:** SPECT; simultaneous dual-isotope imaging; thallium-201; technetium-99m-pyrophosphate

**J Nucl Med 1996; 37:781–785**

The advent of new radiopharmaceuticals such as $^{99m}$Tc myocardial perfusion imaging agents and $^{123}$I-labeled compounds has provoked interest in simultaneously acquired dual-isotope imaging. This technique is advantageous because it can shorten the total acquisition time and reduce errors induced by image misalignment. In spite of these advantages, dual-isotope approaches could potentially cause images derived from the energy window of one radioisotope to be contaminated by spillover from the other tracer (downscatter). Analytical data regarding this downscatter in a clinical setting is limited (*1*). Yet simultaneous $^{201}$Tl/$^{99m}$Tc-pyrophosphate dual-isotope SPECT has been commonly used in patients with acute myocardial infarction (MI) for diagnosing the location and size of infarctions without any downscatter correction.

Since $^{201}$Tl-chloride concentrates in normally perfused myocardium and $^{99m}$Tc-pyrophosphate concentrates in infarct zones, it might have been predicted that downscatter would not present a problem for this particular usage. The purpose of this study is to quantify the degree of the influence of $^{99m}$Tc downscatter on $^{201}$Tl images in simultaneously acquired $^{201}$Tl/$^{99m}$Tc-pyrophosphate dual-isotope SPECT imaging in patients with acute myocardial infarction (MI).

## MATERIALS AND METHODS

### Patients

Thirty-two patients with acute MI who had been referred to our hospital between March 1991 and March 1992 were enrolled into this study. The patients with transmural MI were defined by the

Received Apr. 14, 1995; revision accepted Aug. 17, 1995.

For correspondence or reprints contact: Takaya Fukuyama, MD, Division of Cardiology, Matsuyama Red Cross Hospital, 1 Bunkyou-chou, Matsuyama, Ehime, 790, Japan.

following criteria: (a) a history of chest pain lasting >30 min; (b) electrocardiographic new Q-waves or ST elevation of at least 2 mm in two or more adjacent leads; (c) enzymatic changes typical of acute MI; (d) the presence of a persistent perfusion defect corresponding to the location of the acute MI in a $^{201}$Tl SPECT performed during the chronic phase; and (e) no history of prior MI. Fifteen patients were excluded as with nontransmural MI by this criteria. Therefore, 17 patients (14 men, 3 women; mean age 61 ± 14 yr) with acute "transmural" MI were included in this study. Eleven patients had anterior, two had lateral and four had inferior MI. All subjects gave informed consent.

### Study Protocol

SPECT studies were performed 3 ± 2 days (range 1 to 7 days) after the onset of acute MI. First, 111 MBq $^{201}$Tl were injected intravenously. Ten minutes after the $^{201}$Tl injection, SPECT was performed with a single $^{201}$Tl photopeak window (early $^{201}$Tl image). After SPECT imaging, 740 MBq $^{99m}$Tc-pyrophosphate were injected intravenously. Three hours later, a second $^{201}$Tl image (dual $^{201}$Tl image) and a $^{99m}$Tc image were obtained simultaneously with both $^{201}$Tl and $^{99m}$Tc energy windows. Twenty-four hours after the $^{99m}$Tc injection, another $^{201}$Tl image was obtained with a single $^{201}$Tl photopeak window (24-hr $^{201}$Tl image).

All subjects underwent exercise $^{201}$Tl SPECT imaging during the chronic phase (32 ± 9 days after the onset of acute MI), and all short-axis, vertical long-axis and horizontal long-axis tomograms were interpreted visually by experienced observers.

### SPECT Acquisition and Processing Protocol

All studies were performed using a single-head rotating gamma camera. The large field of view scintillation camera equipped with 37 photomultiplier tubes, a 0.25 in. thick NaI (Tl) crystal and a low-energy, high-resolution, parallel-hole collimator was used in all SPECT acquisitions. Thirty-two projections were obtained in a 180° arc extending from the 60° right anterior oblique to the left posterior oblique projection. For the early and 24-hr $^{201}$Tl imaging, a 25% symmetric energy window centered on the 70–80 keV peak of $^{201}$Tl was used. Dual SPECT acquisition used a 15% symmetric energy window over the 140 keV $^{99m}$Tc photopeak (140 ± 11 keV) and a 25% symmetric window over the 70–80 keV $^{201}$Tl photopeak. The acquisition time per angle was 30 sec for the early $^{201}$Tl imaging and dual imaging, and 45 sec for the 24-hr $^{201}$Tl imaging. All projections were stored as 64 × 64 matrices on disk with a nuclear medicine computer system.

Projection data were not prefiltered. Tomographic reconstructions were performed by a filtered back projection method with a Shepp and Logan Filter using a convolution reconstruction algorithm. The reconstructed transverse axial tomograms (6.0 mm) encompassed the entire heart. These were then nine-point smoothed (4-2-1 weighting) to optimize $^{201}$Tl images. Vertical long-axis and short-axis tomograms parallel to the long and short axes of the left ventricle were extrapolated from the transaxial tomograms by performing a coordinate transformation with appropriate interpolation (*2*). No attenuation or scatter correction was performed.

### Quantification of Myocardial Infarction in Thallium-201 SPECT

Quantification of $^{201}$Tl SPECT images was performed using a method modified from Garcia et al. (*3*) and DePasquale et al. (*4*). Using the vertical long-axis slice with the largest cavity length, the operator selected the short-axis slices for the following quantification. Approximately eight slices, each 6 mm thick, were obtained from each heart. Maximal-count circumferential profiles for each short-axis cut were then automatically generated. These short-axis circumferential profiles were mapped into a two-dimensional polar representation (bull's-eye display).

Since there was no clinically available generated normal limits for Japanese patients, normal files were developed from 20 subjects who were considered normal by probability analysis with normal ECG, normal physical examination and no history of angina or infarction. The normal limit of each profile of bull's-eye display was defined as the curve representing 2.5 s.d. below the mean and was used as the threshold for defect detection.

To quantify MI, two types of polar maps were generated. First, the fraction of infarcted myocardium in a left ventricle (LV) was computed as the percentage of LV pixels representing points which had fallen below normal within the bull's-eye plot, and was defined as the extent score. Secondly, the areas enclosed between the circumferential profile curve below normal and the normal curve were calculated in all short-axis slices of the heart and then summed. This value was divided by the total number of points constructing the bull's-eye display and defined as the severity score.

### Grading of Technetium-99m-pyrophosphate Uptake in Infarct

All planar $^{99m}$Tc images were obtained using a gamma camera with the same low-energy, high-resolution, parallel-hole collimator. Images were obtained in anterior, left anterior oblique and lateral projections 3 hr after the $^{99m}$Tc injection by recording 500,000 counts. Technetium-99m SPECT images were also obtained as described above.

The uptake of $^{99m}$Tc-pyrophosphate in the region of MI was graded from zero to 4+, depending on the $^{99m}$Tc activity over the myocardium on both planar and SPECT images. Zero represents no activity on either planar or SPECT images; 1+ indicated questionable activity on the planar image but was considered definite on the SPECT image; 2+ was considered to be definite on both images where the activity was less intensive than that of the surrounding ribs; 3+ and 4+ represents increased activity within the myocardial image. 3+ represents the activity almost equal to that of the ribs; 4+ represents remarkable accumulation of $^{99m}$Tc-pyrophosphate.

### Statistical Analysis

All values are presented as mean ± s.d. ANOVA was applied to assess the data. When the ANOVA demonstrated a statistically significant result, a Bonferroni's t-test was used to identify the subgroup difference. The level of statistical significance was considered to be $p < 0.05$.

## RESULTS

### Influence of Technetium-99m Downscatter on Thallium-201 Defect

Total image counts of early, dual- and 24-hr $^{201}$Tl images were 200,000 ~ 500,000 counts per projection and the average myocardial counts were 5.4 ± 1.1, 4.6 ± 0.9 and 2.4 ± 0.7 cps/pixel, respectively.

The extent and severity scores obtained from the three sets of $^{201}$Tl images of all study patients are shown in Figure 1. The extent scores calculated from early $^{201}$Tl images and 24-hr $^{201}$Tl images were similar (Fig. 1, top). The extent scores, however, from simultaneous dual-isotope imaging were significantly decreased in all patients ($p < 0.01$, versus early and 24-hr $^{201}$Tl images, for both). Similar results were also obtained for the severity score (Fig. 1, bottom).

Figure 2 shows mean values of the extent and severity scores calculated from the three sets of $^{201}$Tl images, when the scores of early $^{201}$Tl images were standardized to be 100%. The standardized extent score of the 24-hr $^{201}$Tl image was 100% ±

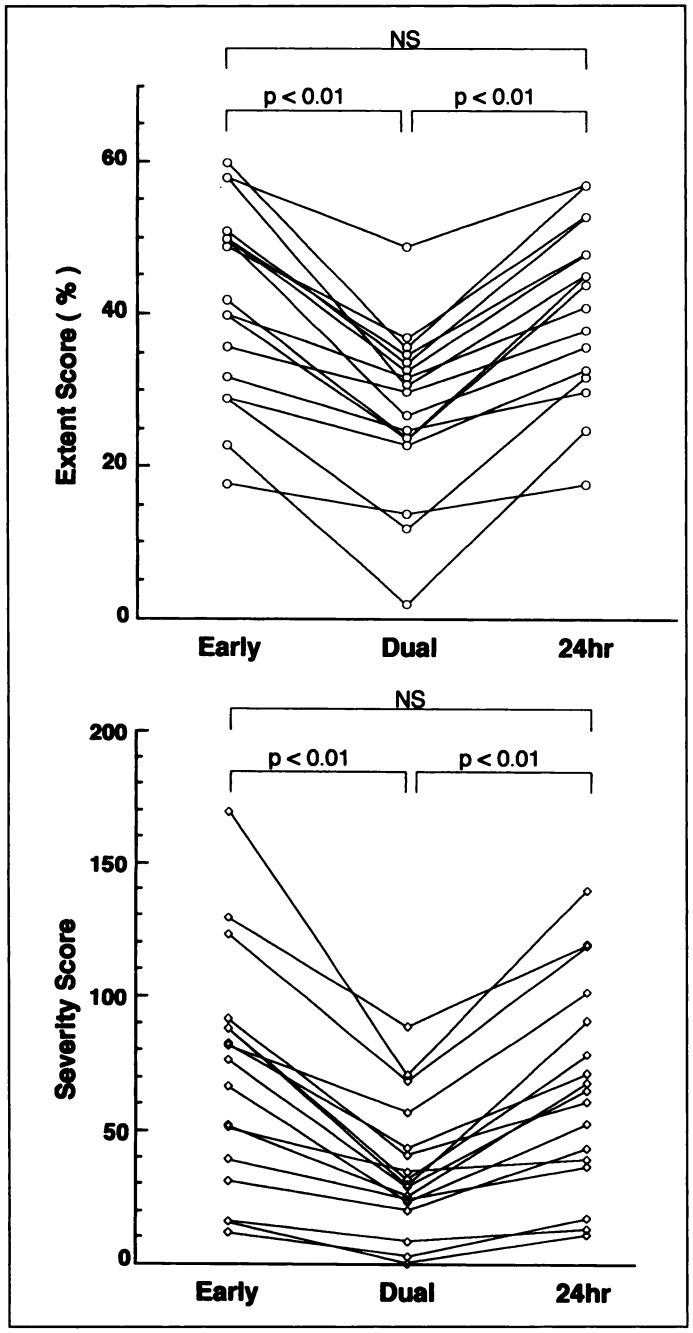


**FIGURE 1.** Actual extent and severity scores obtained from three sets of $^{201}$Tl SPECT images from each patient. Scores were decreased in the dual images in all patients, while they were identical in the early and the 24-hr images.

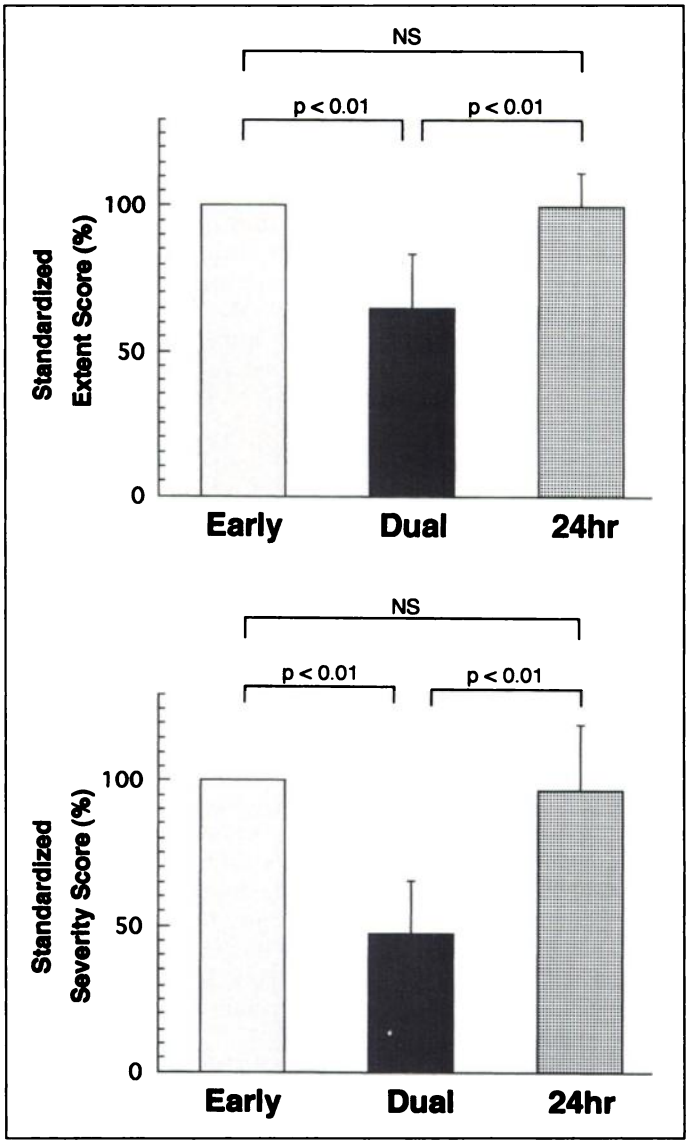


**FIGURE 2.** Standardized extent and severity scores obtained from three sets of $^{201}$Tl SPECT images when both of the early image scores were standardized at 100%. The extent and severity from the dual images were decreased by 36% and 53%, respectively.

11% (NS, versus early $^{201}$Tl image). The extent score of the dual $^{201}$Tl images, however, was 64% ± 19% ($p < 0.01$, versus both the early and the 24-hr $^{201}$Tl images, Fig. 2, top). The standardized severity score of the 24-hr $^{201}$Tl images was 97% ± 23% (NS, versus early $^{201}$Tl image), whereas the severity score of the dual $^{201}$Tl image was only 47% ± 18% ($p < 0.01$, versus both the early and 24-hr $^{201}$Tl images).

### Degree of Accumulation in Myocardial Infarct and Thallium-201

Figure 3 shows the relationship between the change in the extent and severity scores from early to dual-isotope $^{201}$Tl imaging and the degree of accumulation of $^{99m}$Tc-pyrophosphate over infarcted myocardium. There was a tendency for the degree of the change in the extent score to increase, in proportion to the degree of accumulation of $^{99m}$Tc-pyrophosphate (Fig. 3, left). The severity scores decreased significantly

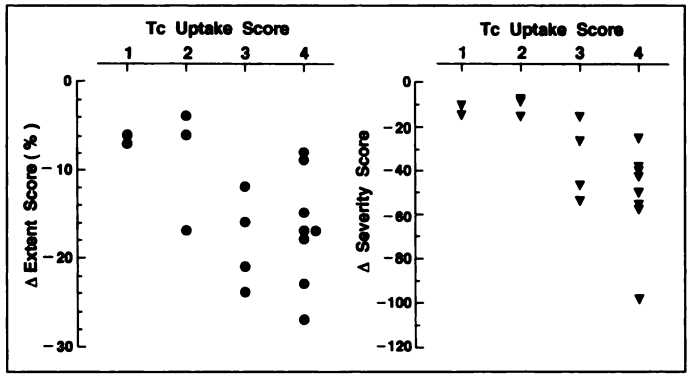


**FIGURE 3.** Relationship between the degree of $^{99m}$Tc accumulation in myocardial infarct and the change in extent and severity scores from early to dual $^{201}$Tl imaging. ΔExtent and Δseverity scores represent the change from early to dual $^{201}$Tl imaging in the extent and the severity scores, respectively.

in proportion to the degree of $^{99m}$Tc accumulation ($p < 0.05$, Fig. 3, right).

*Case Example.* A representative case is shown in Figure 4. A patient with anteroseptal-apical transmural MI underwent the study 2–3 days after its onset. In the early and 24-hr $^{201}$Tl images, a perfusion defect was visible at the anteroapical and septal portion of the left ventricle. These two images were considered identical. In the simultaneous dual-isotope image, however, there was apparently an increased uptake of $^{201}$Tl in the anteroapical and septal portion, corresponding to the location of accumulation of $^{99m}$Tc-pyrophosphate. In particular, the septal portion appeared to be normal in the dual $^{201}$Tl image, and "fill-in" had seemingly occurred in the simultaneous dual-isotope image.

## DISCUSSION

We investigated the effect of $^{99m}$Tc downscatter on the $^{201}$Tl images in simultaneously acquired dual-isotope $^{201}$Tl/$^{99m}$Tc-pyrophosphate imaging in patients with acute MI. The infarct size and its severity obtained from $^{201}$Tl images of dual-isotope imaging were decreased by 36% and 53%, respectively, in comparison with those of $^{201}$Tl SPECT images in which $^{99m}$Tc downscatter was considered to be absent or minimal (early and 24-hr $^{201}$Tl images). The downscatter from $^{99m}$Tc to $^{201}$Tl activity was considerable in simultaneous dual-isotope imaging and was considered to be an inevitable problem when this technique is introduced to clinical use.

In order to evaluate the effect of $^{99m}$Tc downscatter, SPECT images with and without $^{99m}$Tc downscatter should be taken under the same data acquisition condition and compared with each other. Therefore, all SPECT images of the present study and normal data base were acquired with the same low-energy, high-resolution collimator. The numbers of counts acquired in all $^{201}$Tl images were large enough to obtain reasonable SPECT images (*5*).

In this study, we focused on the influence of $^{99m}$Tc downscatter on the $^{201}$Tl acquisition windows because $^{201}$Tl downscatter into the $^{99m}$Tc acquisition window is considered to be very small in a clinical situation, when $^{201}$Tl and $^{99m}$Tc are used as tracers in dual-isotope SPECT imaging (*1,6–8*). In addition to the initial $^{201}$Tl SPECT images, $^{201}$Tl SPECT imaging was performed 24 hr after the $^{99m}$Tc-pyrophosphate injection, in order to obtain $^{201}$Tl SPECT images without contamination of $^{99m}$Tc downscatter and to confirm whether the MIs of study patients were transmural. Twenty-four hours is considered to be sufficient in this patient with these injected activities.

### CAD and Simultaneous Dual-Isotope Imaging

Although $^{201}$Tl SPECT imaging has several drawbacks in determining the infarct size in clinical settings, it has been used for this purpose due to the availability of $^{201}$Tl (*9–11*). Our results showed that $^{201}$Tl SPECT image acquired from simultaneous dual-isotope $^{201}$Tl/$^{99m}$Tc-pyrophosphate imaging significantly underestimate myocardial infarct size.

Even though $^{99m}$Tc-labeled perfusion imaging agents have become available for detecting CAD, $^{201}$Tl imaging is one of the most important tools for the detection of myocardial viability (*12,13*). The segments with mild-to-moderately reduced thallium activities have been confirmed to be metabolically active (*13*) and improve functionally after coronary artery bypass graft surgery (CABG) (*12*). Our data showed that the severity of $^{201}$Tl defects diminished by more than 50% in the presence of $^{99m}$Tc scatter contribution. The extent to which the $^{201}$Tl activity apparently increased is enough for us to erroneously overestimate myocardial viability and to lead to unnecessary interventions, such as coronary angioplasty or CABG.

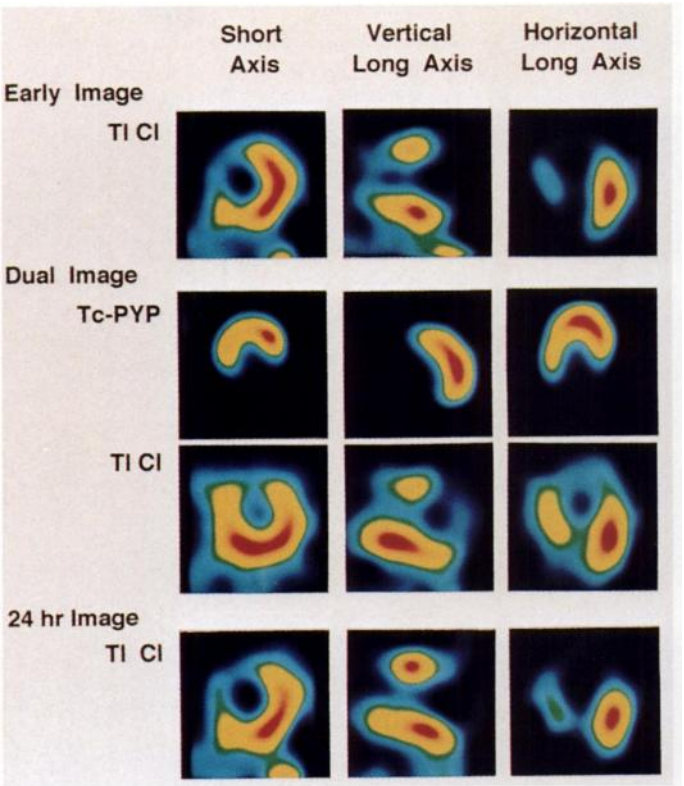


**FIGURE 4.** A representative case of simultaneous $^{201}$Tl/$^{99m}$Tc dual-isotope imaging. This patient had anteroseptal and apical transmural myocardial infarction. The septal portion of the left ventricle appears to be filled-in in dual $^{201}$Tl imaging compared to early or 24-hr imaging.

Lowe et al. (*14*) used a phantom study to address the feasibility of simultaneous rest $^{201}$Tl/stress $^{99m}$Tc-sestamibi dual-isotope SPECT. They reported only a 10% reduction in the myocardium-to-defect count ratio in dual $^{201}$Tl imaging as a result of $^{99m}$Tc downscatter. Kiat et al. (*1*) also investigated the feasibility of the dual-isotope myocardial perfusion SPECT protocol in patients with CAD using $^{201}$Tl/$^{99m}$Tc-sestamibi simultaneously. They concluded that simultaneous dual-isotope protocols, however, were not feasible for detecting CAD because of the presence of the substantial amount of the $^{99m}$Tc downscatter into $^{201}$Tl windows.

In the present study we showed that $^{99m}$Tc downscatter into $^{201}$Tl windows was substantial. The protocol that we used to assess the degree of $^{99m}$Tc downscatter into $^{201}$Tl windows might be different from those of the $^{201}$Tl/$^{99m}$Tc-sestamibi studies since $^{201}$Tl concentrates in normal areas and $^{99m}$Tc-pyrophosphate concentrates in infarct areas. Nevertheless, our result also implies that a considerable amount of $^{99m}$Tc downscatter is present within the $^{201}$Tl windows.

### Attempts for Downscatter Compensation

To date, several procedures for the downscatter compensation have been proposed. Hashimoto et al. suggested that it is possible to compensate for the downscatter of each isotope into nonprimary energy window through the use of simple formulas in simultaneously acquired dual-isotope $^{201}$Tl/$^{99m}$Tc-pyrophosphate imaging in patients with acute MI (*15*). Neumann also applied the same procedure to the compensation for the downscatter to detect and characterize parathyroid pathology (*16*). Nakashima et al. examined the ratio of the count of an isotope in different windows in simultaneous $^{201}$Tl/$^{123}$I dual-isotope SPECT in clinical settings and reported that this ratio was not

uniform (*17*). This implies that the procedure assuming a fractional contribution from an isotope into another isotope window is not appropriate in the clinical setting. Sorenson and Phelps described that the technique is not reliable for in vivo measurements because of varying amounts of downscatter due to Compton scattering within body (*18*).

Ichihara et al. (*19*) proposed a triple-energy window scatter compensation method for determining Compton scatter and validated the applicability of this technique to the downscatter correction in dual-isotope SPECT in phantom study. This method may be useful because downscatter correction can be performed on pixel-by-pixel basis and in individual cases. An energy-weighted acquisition technique to obtain different isotope data sets in simultaneous dual-isotope acquisition has also been proposed (*20*). The clinical applicability of these techniques are still preliminary.

Weinstein et al. first imaged the $^{99m}$Tc source in dual $^{201}$Tl/$^{99m}$Tc windows, followed by $^{201}$Tl administration and dual-isotope imaging (*8*). The $^{99m}$Tc image in the $^{201}$Tl window was subtracted from the dual $^{201}$Tl image to specifically correct for the $^{99m}$Tc downscatter. In the tracer combination such as $^{99m}$Tc and $^{201}$Tl in dual imaging, this would be useful if precise pixel registration between the two different images were ensured in the clinical setting. In case employing lead collimator in data acquisition, there may be a large contribution of lead x-ray from $^{99m}$Tc scatter within $^{201}$Tl photopeak. With use of a different collimator, it may be possible to eliminate this kind of scatter contribution in dual isotope imaging.

## CONCLUSION

The present study documents that $^{99m}$Tc downscatter into $^{201}$Tl windows greatly contribute to $^{201}$Tl images in simultaneously acquired dual-isotope $^{201}$Tl/$^{99m}$Tc-pyrophosphate imaging. The amount of $^{99m}$Tc downscatter in the simultaneous dual-imaging approach is considerable enough to result in misinterpretation in determining infarct size and myocardial viability. This protocol awaits validation of methods to correct for downscatter.


## ACKNOWLEDGMENTS

We thank Akio Hiraoka and Takeshi Hisa of the Nuclear Medicine Section, Matsuyama Red Cross Hospital, for their excellent technical support and Ms. Akemi Hirano for administrative assistance.


## REFERENCES


1. Kiat H, Germano G, Friedman J, et al. Comparative feasibility of separate or simultaneous rest thallium-201/stress technetium-99m-sestamibi dual-isotope myocardial perfusion SPECT. *J Nucl Med* 1994;35:542–548.
2. Borrello JA, Clinthorne NH, Rogers WL, Thrall JH, Keyes JW. Oblique-angle tomography: a restructuring algorithm for transaxial tomographic data. *J Nucl Med* 1981;22:471–473.
3. Garcia EV, Van Train K, Maddahi J, et al. Quantification of rotational thallium-201 myocardial tomography. *J Nucl Med* 1985;26:17–26.
4. DePasquale EE, Nody AC, DePuey EG, et al. Quantification rotational thallium-201 tomography for identifying and localizing coronary artery disease. *Circulation* 1988;77:316–327.
5. Sorenson JA, Phelps ME. Nuclear medicine tomography: systems and devices. In: Sorenson JA, Phelps ME, eds. *Physics in Nuclear Medicine,* 2nd ed. Philadelphia: Saunders 1987;424–451.
6. Kiat H, Germano G, Van Train K, et al. Quantitative assessment of photon spillover in simultaneous rest $^{201}$Tl/stress $^{99m}$Tc-sestamibi dual-isotope myocardial perfusion SPECT [Abstract]. *J Nucl Med* 1992;33:854.
7. Weinstein H, Hademenos G, Reinhardt CP, McSherry B, Wironen J, Leppo JA. A new method of simultaneous dual isotope $^{99m}$Tc/$^{201}$Tl imaging and spilldown correction [Abstract]. *Circulation* 1992;86 (suppl):I–707.
8. Weinstein H, King MA, Reinhardt CP, McSherry BA, Leppo JA. A method of simultaneous dual-radionuclide cardiac imaging with technetium-99m and thallium-201. I. Analysis of interradionuclide crossover and validation in phantoms. *J Nucl Cardiol* 1994;1:39–51.
9. Tamaki S, Nakajima H, Murakami T, et al. Estimation of infarct size by myocardial emission computed tomography with thallium-201 and its relation to creatine kinase-MB release after myocardial infarction in man. *Circulation* 1982;66:994–1001.
10. Wolfe CL, Lewis SE, Corbett JR, Parkey RW, Buja M, Willerson JT. Measurement of myocardial infarction fraction using single-photon emission computed tomography. *J Am Coll Cardiol* 1985;6:145–151.
11. Prigent F, Maddahi J, Garcia EV, Satoh Y, Van Train K, Berman DS. Quantification of myocardial infarct size by thallium-201 single-photon emission computed tomography: experimental validation in the dog. *Circulation* 1986;74:852–861.
12. Ragosta M, Beller GA, Watson DD, Kaul S, Gimple LW. Quantitative planar rest-redistribution $^{201}$Tl imaging in detection of myocardial viability and prediction of improvement in left ventricular function after coronary bypass surgery in patients with severely depressed left ventricular function. *Circulation* 1993;87:1630–1641.
13. Dilsizian V, Perrone-Filardi P, Arrighi JA, Bacharach SL, Quyyumi AA, Freedman NMT, Bonow RO. Concordance and discordance between stress-redistribution-reinjection and rest-redistribution thallium imaging for assessing viable myocardium. Comparison with metabolic activity by positron emission tomography. *Circulation* 1993;88:941–952.
14. Lowe VJ, Greer KL, Hanson MW, Jaszczak RJ, Coleman RE. Cardiac phantom evaluation of simultaneously acquired dual-isotope rest thallium-201/stress technetium-99m SPECT images. *J Nucl Med* 1993;34:1998–2006.
15. Hashimoto T, Kambara H, Fudo T, et al. Significance of technetium-99m/thallium-201 overlap on simultaneous dual emission computed tomography in acute myocardial infarction. *Am J Cardiol* 1988;61:1181–1186.
16. Neumann DR. Simultaneous dual-isotope SPECT imaging for the detection and characterization of parathyroid pathology. *J Nucl Med* 1992;33:131–134.
17. Nakashima K, Taki J, Bunko H, et al. Error of uptake in dual energy acquisition with $^{201}$Tl and $^{123}$I-labeled radiopharmaceuticals. *Eur J Nucl Med* 1990;16:595–599.
18. Sorenson JA, Phelps ME. Counting system-Part 1. In: Sorenson JA, Phelps ME, eds. *Physics in Nuclear Medicine,* 2nd ed. Philadelphia: Saunders 1987;261–279.
19. Ichihara T, Ogawa K, Motomura N, Kubo A, Hashimoto S. Compton scatter compensation using the triple-energy window method for single- and dual-isotope SPECT. *J Nucl Med* 1993;34:2216–2221.
20. Hasselquist BE, Boudreau RJ, Kuni CC, duCret RP, DeVito R. Experimental verification of energy weighted dual-isotope technique for simultaneous $^{201}$Tl/$^{99m}$Tc SPECT cardiac imaging [Abstract]. *J Nucl Med* 1993;34:108.